J Comput Electron (2017) 16:90–97
DOI 10.1007/s10825-016-0935-x

Application of generalized logistic functions in surface-potential-based MOSFET modeling

Tijana Kevkić[1] · **Vladica Stojanović**[1] · **Dušan Joksimović**[2]

Published online: 24 November 2016

Abstract An improved surface-potential-based metal–oxide–semiconductor field-effect transistor (MOSFET) model is presented. The improvement consists in introducing a new generalized logistic functional form for the smoothing factor that allows for a continuous transition of the surface potential from the depletion to strong inversion region. This functional form takes into account specific changes in the technological characteristics of MOSFET devices. The model combines the advantages of both regional and single-piece models and satisfies all requirements for compact models, i.e., continuity, accuracy, scalability, and simulation performance. Comparison with numerical data shows that the model provides an accurate description of the surface potential for a wide range of substrate doping and oxide thickness.

Keywords MOSFET modeling · Generalized logistic functions · Surface potential · Parameter estimation

✉ Vladica Stojanović
vladica.stojanovic@pr.ac.rs

Tijana Kevkić
tijana.kevkic@pr.ac.rs

Dušan Joksimović
dusan.joksimovic@kpa.edu.rs

[1] Faculty of Science and Mathematics, Lole Ribara 29, 40000 Kosovska Mitrovica, Serbia

[2] Academy of Criminalistics and Police Studies, Cara Dušana 196, 11000 Belgrade, Serbia

1 Introduction

Surface-potential-based models (SPBMs) are among the most accurate and physically based compact MOSFET models available today. They provide an accurate and continuous description of the current and its derivatives in all operating regions [1]. However, SPB models have been avoided for a long time because the surface potential is given implicitly in terms of the terminal voltages and so can only be solved iteratively [2,3]. This places a severe computational burden on compact MOSFET models. To overcome this difficulty, an approximate explicit relation between the surface potential and gate voltage was developed in [4].

Unfortunately, the accuracy of that approximation is about 2–3 mV [5], which does not permit accurate reproduction of derivatives of current and charges in the moderate inversion region. On the other hand, due to scaling of complementary metal–oxide–semiconductor (CMOS) technology, use of MOS transistors is increasingly being restricted to low-voltage and low-current regimes [6]. Gate bias conditions around the threshold voltage are more commonplace, and MOS transistors are used principally in the moderate inversion region, where the proposed explicit model is least accurate [7].

Bearing this in mind, we improved the original explicit SPB model [4] by introducing the *generalized logistic* (GL) fitting function into the corresponding expression for the surface potential. A pure empirical smoothing factor for the transition function of the original model is thereby replaced by the GL-fit factor, which can be precisely determined for given technological characteristics of the MOSFET device. This approach enables control of the smoothness as well as speed of the surface potential transition from the depletion to strong inversion region. The simulated values of surface potential match closely with numerical

solutions of the mentioned well-known implicit relation for a wide range of substrate doping and oxide thickness.

2 Explicit SPB model

Consider an n-type MOS transistor with gate oxide thickness t_{ox} and channel region homogeneously doped to acceptor concentration of N_A. Adopting the gradual channel and charge sheet approximations, for the useful range of an n-type MOS transistor, the electrostatic surface potential ψ_s can be calculated from the following implicit relation [8]:

$$V_G - V_{FB} - \psi_s = \gamma \sqrt{\psi_s + u_T \exp\left(\frac{\psi_s - 2\phi_F - V_{ch}}{u_T}\right)}, \quad (1)$$

where V_{FB} is the flat-band voltage, $u_T = kT/q$ is the thermal voltage, ϕ_F is the bulk potential, $\gamma = \sqrt{2q\varepsilon_{Si}N_A}/C_{ox}$ is the body effect coefficient in which $C_{ox} = \varepsilon_{ox}/t_{ox}$ is the gate oxide capacitance per unit area, and V_{ch} is the channel potential defined by the difference between the quasi-Fermi potential of the carriers forming the channel (ϕ_n) and that of the majority carriers (ϕ_p).

From Eq. (1), it is clear that ψ_s cannot be found explicitly as a function of V_G and has to be solved numerically. In [4], an explicit approximate solution of Eq. (1) was developed for $\psi_s > 0$, expressed as

$$\psi_s^*(V_G) = f + u_T \ln\left\{\frac{1}{\gamma^2 u_T}\left[V_G - V_{FB} - f - \frac{\psi_{s_{wi}} - f}{\sqrt{1 + \left(\frac{\psi_{s_{wi}} - f}{4u_T}\right)^2}}\right]^2 - \frac{f}{u_T} + 1\right\}, \quad (2)$$

where $\psi_{s_{wi}}$ is the surface potential in the weak inversion region, where the inequality $\psi_s < 2\phi_F + V_{ch}$ holds. In this case, the exponential term in Eq. (1) is negligible, and the surface potential can be approximately written as follows [4]:

$$\psi_{s_{wi}} = \left(-\frac{\gamma}{2} + \sqrt{V_G - V_{FB} + \frac{\gamma^2}{4}}\right)^2. \quad (3)$$

In addition, the empirical function f in Eq. (2) should change value smoothly from $\psi_{s_{wi}}$ to $2\phi_F + V_{ch}$, as given by [4,9]

$$f = \frac{2\phi_F + V_{ch} + \psi_{s_{wi}}}{2} - \frac{1}{2}\sqrt{\left(\psi_{s_{wi}} - 2\phi_F - V_{ch}\right)^2 + 4\varepsilon^2}. \quad (4)$$

The smoothing factor ε enables a smooth transition of the function f from the weak inversion region to the onset of the strong inversion region. Its value was initially fixed at a convenient value of 0.02 V [4].

3 GL modification of the factor ε

The function f given by Eq. (4) should reduce (approximately) to $\psi_{s_{wi}}$ for $V_G < V_T$, where V_T is the threshold voltage defined with respect to V_{ch} and is given by

$$V_T = V_G\Big|_{\psi_s = 2\phi_F + V_{ch}} = V_{FB} + 2\phi_F + V_{ch} + \gamma\sqrt{2\phi_F + V_{ch}}.$$

However, deep in the weak inversion region, f as given by Eq. (4) still remains a function of V_{ch}, and its value significantly differs from $\psi_{s_{wi}}$. This difference decreases with a decreasing value of the smoothing factor ε in the subthreshold region. To bring the values of the function f closer to the value of $\psi_{s_{wi}}$, a reduction of the value of ε in the subthreshold region is needed. Unfortunately, simply setting ε to zero would make the transition of the function f abrupt at the threshold voltage, jeopardizing the smoothness of the behaviors of both f and ψ_s^* as functions of the effective voltage $V_E = V_G - V_T$. To avoid this, the constant value of the factor ε should be replaced by a function which varies from a value close to zero in the depletion region, to a value close to 0.02 V as the threshold voltage V_T is approached. For this purpose, the following form for the factor ε as a function of the effective bias V_E was proposed in [10]:

$$\varepsilon_m(V_E) = 0.01\left(1 + \frac{V_E + 8u_T}{\sqrt{(V_E + 8u_T)^2 + 0.02}}\right). \quad (5)$$

Values of ψ_s^* obtained from Eq. (2) and with ε given by Eq. (5) show better agreement with the numerical results of the implicit Eq. (1) compared with the constant value of 0.02 V, as proposed in [4].

On the other hand, several simulations have shown that values of ψ_s^* obtained using ε_m deviate significantly from the results of the implicit SPB model, especially for thin gate oxide and high dopant concentration in MOSFETs [11]. These deviations are due to the purely empirical nature of the function $\varepsilon_m(V_E)$ in Eq. (5), which does not take into account changes in the specific technological characteristics of MOSFET devices. In particular, the type and speed of the transition of the factor ε from 0 to 0.02 are sensitive to changes in the device's technological characteristics. This further means that the transition of the function f, and consequently of ψ_s^*, between weak and strong inversion is dependent on the device's technological characteristics.

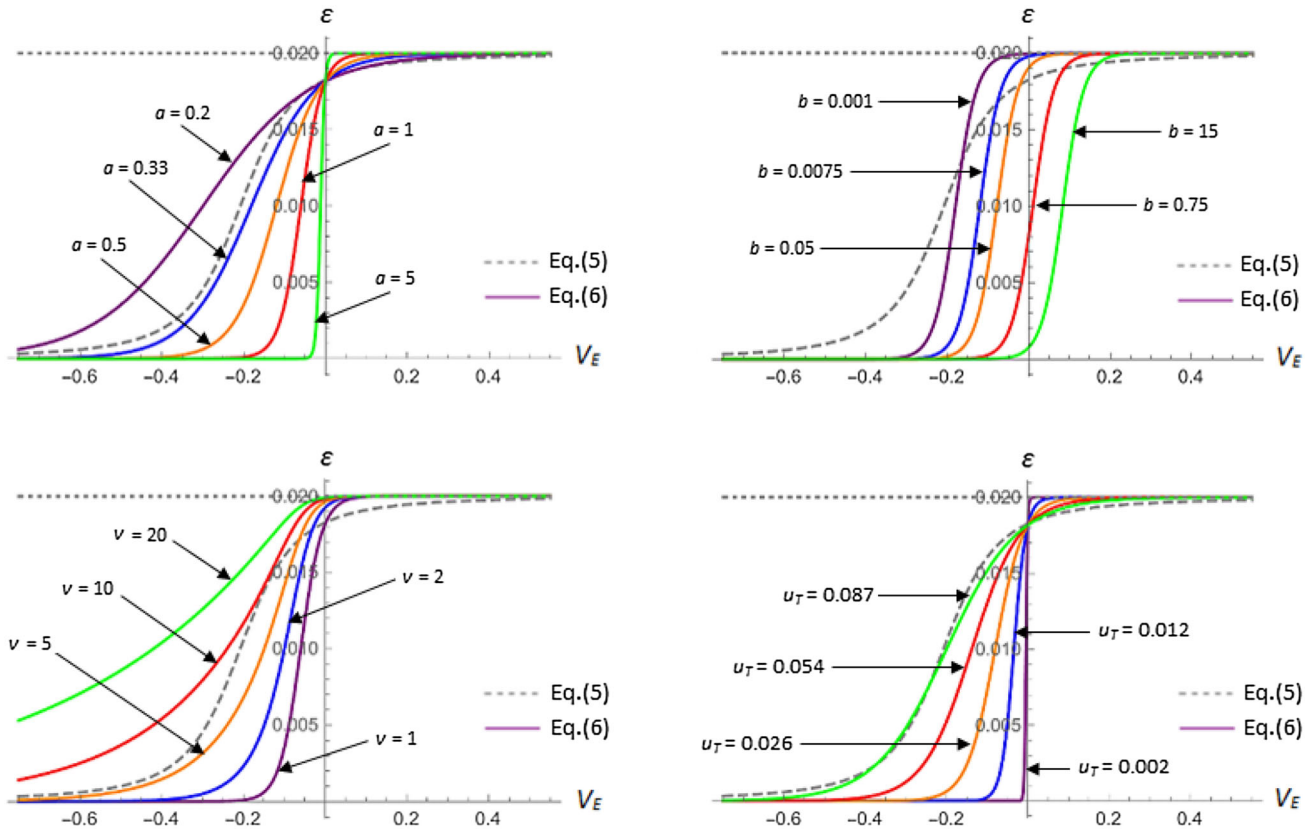

Fig. 1 GL-fit factor ε versus effective voltage V_{E}, using Eq. (6) (*solid lines*), compared with the fitting model proposed in Eq. (5) (*dashed line*). *Upper left diagram* variation of the parameter a ($b = 0.1$, $\nu = 1$, $u_{\mathrm{T}} = 0.026$). *Upper right diagram* variation of the parameter b ($a = \nu = 1$, $u_{\mathrm{T}} = 0.026$). *Lower left diagram* variation of the parameter ν ($a = 1$, $b = 0.1$, $u_{\mathrm{T}} = 0.026$). *Lower right diagram* variation of the parameter u_{T} ($a = \nu = 1$, $b = 0.1$)

Based on these considerations, the following *generalized logistic* (GL) functional form for ε is proposed herein:

$$\varepsilon_{\mathrm{GL}}(V_{\mathrm{E}}) = 0.02\left[1 + b\,\exp\left(-a\frac{V_{\mathrm{E}}}{u_{\mathrm{T}}}\right)\right]^{-1/\nu}, \tag{6}$$

where a, b, $\nu > 0$ are the GL model parameters. For $0 < \varepsilon_{\mathrm{GL}}(V_{\mathrm{E}}) < 0.02$, it holds that

$$\frac{\mathrm{d}\varepsilon_{\mathrm{GL}}(V_{\mathrm{E}})}{\mathrm{d}V_{\mathrm{E}}} = \frac{a}{\nu u_{\mathrm{T}}}\left[1 - \left(\frac{\varepsilon_{\mathrm{GL}}(V_{\mathrm{E}})}{0.02}\right)^{\nu}\right]\varepsilon_{\mathrm{GL}}(V_{\mathrm{E}}) > 0. \tag{7}$$

Thus, the growth of the $\varepsilon_{\mathrm{GL}}$ value depends directly on a and ν, which are called the growth parameters. On the other hand, the parameter b determines the shift of the GL curve through the relation $\varepsilon_{\mathrm{GL}}(0) = 0.02(1 + b)^{-1/\nu} \lesssim 0.02$. According to the differential equation

$$\frac{\mathrm{d}^2\varepsilon_{\mathrm{GL}}(V_{\mathrm{E}})}{\mathrm{d}V_{\mathrm{E}}^2} = \left(\frac{a}{\nu u_{\mathrm{T}}}\right)^2\left[1 - \left(\frac{\varepsilon_{\mathrm{GL}}(V_{\mathrm{E}})}{0.02}\right)^{\nu}\right] \times\left[1 - (1+\nu)\left(\frac{\varepsilon_{\mathrm{GL}}(V_{\mathrm{E}})}{0.02}\right)^{\nu}\right]\varepsilon_{\mathrm{GL}}(V_{\mathrm{E}}), \tag{8}$$

it follows that the GL curve exhibits its maximum growth at the transition point $V_{\mathrm{SP}} = u_{\mathrm{T}}a^{-1}\ln(b/(2^{\nu} - 1))$, where $\mathrm{d}^2\varepsilon_{\mathrm{GL}}(V_{\mathrm{SP}})/\mathrm{d}V_{\mathrm{E}}^2 = 0$ and $\varepsilon_{\mathrm{GL}}(V_{\mathrm{SP}}) = 0.01$ hold.

According to Eqs. (6–8), it follows that $\varepsilon_{\mathrm{GL}}$, as a function of V_{E}, exhibits a smooth transition from a value close to zero in the weak inversion region, where $V_{\mathrm{E}} < 0$ holds, to its maximum of 0.02, when $V_{\mathrm{E}} \geq 0$. The various types of $\varepsilon_{\mathrm{GL}}$ transition obtained for different values of the parameters a, b, and ν, as well as the thermal voltage u_{T}, are plotted in Fig. 1. Graphs of $\varepsilon_{\mathrm{m}}(V_{\mathrm{E}})$ are also shown in this figure for comparison. As can be seen, simple changes in the values of the GL model parameters can lead to great versatility and adaptability of the transition in the GL-fit values $\varepsilon_{\mathrm{GL}}(V_{\mathrm{E}})$ from 0 to 0.02.

4 Model formulation

The main purpose of this section is estimation of the unknown parameters $a, b > 0$, by using some standard fitting techniques. Unlike them, the third parameter $\nu > 0$ is determined in advance, according to the condition of the asymptotic linear growth

$$y = L(x) = ax - \ln b, \tag{9}$$

where $y = \ln\left(\varepsilon_{\mathrm{GL}}^{\nu}/(0.02^{\nu} - \varepsilon_{\mathrm{GL}}^{\nu})\right)$ and $x = V_{\mathrm{E}}/u_{\mathrm{T}}$. Thanks to the linear form of the function $L(x)$, the factor $\varepsilon_{\mathrm{GL}}$ can be obtained by using a fitting procedure based on the following algorithm:

Step 1 For given values of gate voltage $V_{\mathrm{G}}^{(1)}, \ldots, V_{\mathrm{G}}^{(n)}$, solve Eq. (1) numerically with respect to ψ_{s}, i.e., compute the values $\psi_{\mathrm{s}}^{(1)}, \ldots, \psi_{\mathrm{s}}^{(n)}$ such that

$$V_{\mathrm{G}}^{(k)} - V_{\mathrm{FB}} - \psi_{\mathrm{s}}^{(k)} = \gamma\left[\psi_{\mathrm{s}}^{(k)} + u_{\mathrm{T}}\exp\left(\frac{\psi_{\mathrm{s}}^{(k)} - 2\phi_{\mathrm{F}} - V_{\mathrm{ch}}}{u_{\mathrm{T}}}\right)\right]^{1/2}.$$

Step 2 Find values $f_1, \ldots, f_n$ as the solutions of equations $\psi_{\mathrm{s}}^{(k)} = \psi_{\mathrm{s}}^{*}(V_{\mathrm{G}}^{(k)})$, $k = 1, \ldots, n$.
Step 3 According to Eq. (3), compute, for each $k = 1, \ldots, n$, the values

$$\psi_{\mathrm{s_{wi}}}^{(k)} := \psi_{\mathrm{s_{wi}}}\left(V_{\mathrm{G}}^{(k)}\right),$$
$$\varepsilon_{\mathrm{k}} := \frac{1}{2}\left|\left(2f_k - 2\phi_{\mathrm{F}} - V_{\mathrm{ch}} - \psi_{\mathrm{s_{wi}}}^{(k)}\right)^2 - \left(\psi_{\mathrm{s_{wi}}}^{(k)} - 2\phi_{\mathrm{F}} - V_{\mathrm{ch}}\right)^2\right|^{1/2}.$$

Step 4 Determine the value of the parameter $\nu > 0$ which satisfies the asymptotic linear growth condition in Eq. (9).
Step 5 With respect to $a, b > 0$, minimize the objective function

$$F(a,b) := \sum_{k=1}^{n}\left[L\left(\frac{V_{\mathrm{E}}^{(k)}}{u_{\mathrm{T}}}\right) - \ln\frac{\varepsilon_k^{\nu}}{0.02^{\nu} - \varepsilon_k^{\nu}}\right]^2,$$

where $V_{\mathrm{E}}^{(k)} = V_{\mathrm{G}}^{(k)} - V_{\mathrm{T}}$, $k = 1, \ldots, n$.
Step 6 For estimated values of $a, b > 0$, form the GL-fit factor $\varepsilon_{\mathrm{GL}}(V_{\mathrm{E}})$, as given in Eq. (6).

We remark that the minimization of the function $F(a, b)$ in step 5 is usually performed by using the well-known least-squares approximation method [12], i.e., by solving the coupled equations $\partial F(a,b)/\partial a = \partial F(a,b)/\partial b = 0$. The estimates of the GL model parameters a, b, ν obtained from the described algorithm are presented in Table 1, for two MOS transistors with significantly different technological characteristics. All estimates were computed according to a series of $n = 20$ equidistant values of gate voltage V_{G}, and the whole algorithm was implemented in the software package MATHEMATICA 11.0.0.

Note that the estimated values of the parameters a, ν and the intercept $-\ln b$ are greater for MOSFET B; i.e., reducing t_{ox} as well as increasing N_{A} leads to faster growth of the GL curve. In addition, a larger value of the intercept ensures a decrease of the shift parameter b and satisfaction of the condition $\varepsilon_{\mathrm{GL}}(0) \lesssim 0.02$. Finally, for the two devices considered, the coefficients of determination (R^2) were higher than 99 % and Akaike's information criterion (AIC) coefficient took pronounced negative values. This indicates good performance of the GL-fit factor, $\varepsilon_{\mathrm{GL}}$, as an adequate theoretical model.

Table 1 Estimated values of GL-fit model parameters, according to MOSFET technological characteristics and goodness-of-fit estimated statistics

Item	MOSFET A	MOSFET B
t_{ox} (nm)	2.5	1.2
N_{A} (cm^{-3})	5×10^{17}	5×10^{18}
C_{ox} ($\mathrm{F\,m}^{-2}$)	0.0138	0.0288
$2\phi_{\mathrm{F}}$ (V)	0.9100	1.0416
γ ($\mathrm{V}^{1/2}$)	0.2891	0.4494
V_{FB} (V)	−0.8000	−1.0000
V_{T} (V)	0.3857	0.5002
ν	4.0000	5.500
a	0.6430	0.9676
$\ln b^{-1}$	1.9272	5.0471
b	0.1456	0.0064
$\varepsilon_{\mathrm{GL}}(0)$ (V)	0.0193	0.0200
R^2	0.9996	0.9987
AIC	−23.56	−10.09

The GL-fit factor $\varepsilon_{\mathrm{GL}}$ as a function of V_{E}, obtained by using the proposed algorithm, is plotted in Fig. 2 (solid lines in left diagrams). The real-based values $\varepsilon_1, \ldots, \varepsilon_n$ obtained in step 3 are taken as reference values (dots in Fig. 2). Figure 2 shows an almost exact match between the $\varepsilon_{\mathrm{GL}}$ and reference values. This agreement is obviously better than for ε_{m} (especially for MOSFET B), which is shown by dashed lines in the same figure for comparison. Finally, the linear approximation $y = L(x)$ obtained from Eq. (9) is shown in the right diagrams of Fig. 2.

5 Model validation

The improvement of the original explicit SPB model by introducing the GL function can be clearly seen from Tables 2 and 3, which show the mean values of the absolute error (AE), fractional error (FE), and squared error (SE) for the fitting factor ε, empirical function f, and approximate surface potential ψ_{s}^{*}. Values from the previous algorithm were used as reference, and all errors were computed for two considered MOS transistors, separately for the weak and strong

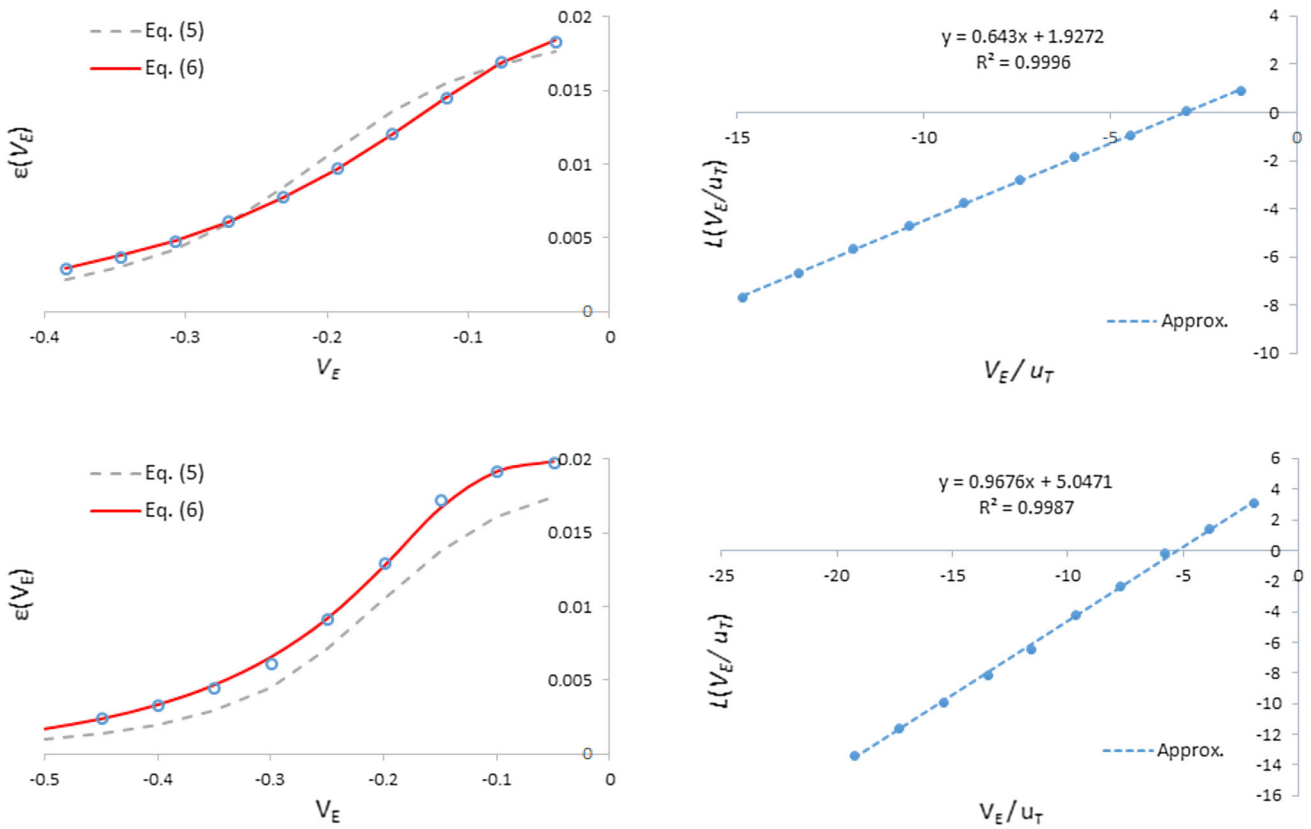

Fig. 2 Estimated values of ε_{m} and $\varepsilon_{\mathrm{GL}}$ versus V_{E} (*left diagrams*) and least-squares approximation of $y = L(x)$ defined in Eq. (9) (*right diagrams*). Device parameters are the same as in MOSFET A (*upper diagrams*) and MOSFET B (*lower diagrams*)

Table 2 Estimated errors when using various types of ε fitting (MOSFET A)

Error	Region	ε-Fitting		f-Fitting		ψ_{s}^{*}-Approx.	
		Eq. (5)	Eq. (6)	Eq. (5)	Eq. (6)	Eq. (5)	Eq. (6)
AE	W.i.	7.29×10^{-4}	6.68×10^{-5}	1.33×10^{-4}	1.65×10^{-5}	1.34×10^{-5}	2.36×10^{-6}
	S.i.	2.50×10^{-2}	2.48×10^{-2}	3.27×10^{-3}	3.25×10^{-3}	2.97×10^{-3}	2.96×10^{-3}
FE (%)	W.i.	1.05×10^{1}	9.00×10^{-1}	1.66×10^{-2}	2.00×10^{-3}	1.58×10^{-3}	2.72×10^{-4}
	S.i.	5.55×10^{1}	5.51×10^{1}	3.61×10^{-1}	3.59×10^{-1}	2.85×10^{-1}	2.83×10^{-1}
SE	W.i.	6.90×10^{-7}	6.05×10^{-9}	4.01×10^{-8}	1.09×10^{-9}	8.98×10^{-10}	3.96×10^{-11}
	S.i.	6.34×10^{-4}	6.26×10^{-4}	1.07×10^{-5}	1.06×10^{-5}	8.85×10^{-6}	8.77×10^{-6}

Table 3 Estimated errors when using various types of ε fitting (MOSFET B)

Error	Region	ε-Fitting		f-Fitting		ψ_{s}^{*}-Approx.	
		Eq. (5)	Eq. (6)	Eq. (5)	Eq. (6)	Eq. (5)	Eq. (6)
AE	W.i.	1.98×10^{-3}	1.58×10^{-4}	7.08×10^{-4}	4.55×10^{-4}	9.21×10^{-5}	7.20×10^{-5}
	S.i.	1.17×10^{-2}	1.15×10^{-2}	1.79×10^{-3}	1.76×10^{-3}	1.05×10^{-2}	1.05×10^{-2}
FE (%)	W.i.	2.79×10^{1}	2.17×10^{0}	7.33×10^{-2}	4.63×10^{-2}	9.30×10^{-3}	7.24×10^{-3}
	S.i.	3.44×10^{1}	3.38×10^{1}	1.72×10^{-1}	1.70×10^{-1}	9.13×10^{-1}	9.11×10^{-1}
SE	W.i.	4.60×10^{-6}	5.91×10^{-8}	2.42×10^{-6}	1.43×10^{-6}	5.92×10^{-8}	4.17×10^{-8}
	S.i.	1.74×10^{-4}	1.68×10^{-4}	3.68×10^{-6}	3.55×10^{-6}	1.27×10^{-4}	1.26×10^{-4}

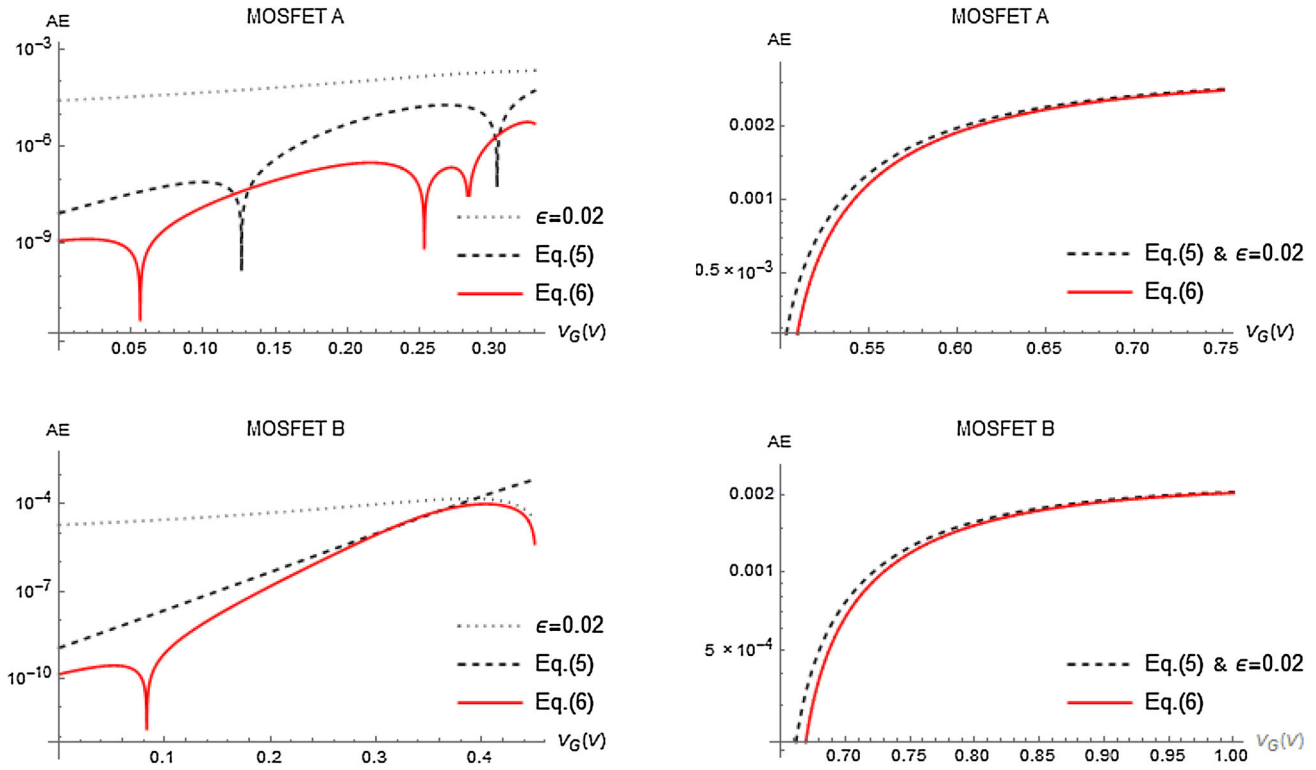

Fig. 3 Log plots of absolute errors of SP approximations ψ_s^* versus V_G, fitted with different factors ε, in the weak inversion (*left diagrams*) and strong inversion region (*right diagrams*). Device parameters are as for MOSFET A (*upper diagrams*) and MOSFET B (*lower diagrams*)

inversion region. As one can see from both tables, all the estimated errors in the case of the GL-fit factor, given by Eq. (6), are smaller than those predicted when using Eq. (5). This is particularly noticeable in the weak inversion region, where, for instance, the FE of the ε fitting is lower by about 13 times compared with when the GL factor ε_{GL} was used. On the other hand, in the strong inversion region, both factors take the conventional value of 0.02. This is why there are not so significant differences between the computed errors, though they are again lower in the case of the factor ε_{GL}.

The AE functions, $\mathrm{AE} = \left|\psi_s^* - \psi_s\right|$ are shown in Fig. 3, on logarithmic scale. The values of ψ_s^* were obtained from Eq. (2) by using ε_m, ε_{GL}, as well as the constant value of 0.02 V, respectively. It is easy to observe that the values of ψ_s^* when using the GL-fit factor ε_{GL} show the lowest deviation from the reference values in all the diagrams.

6 Results for drain current

Another advantage of introducing the GL-fit factor ε_{GL} into the original explicit SPB model is minimization of drift current anomalies in the subthreshold region. According to the charge sheet approximation, the equation for drift current depends on the difference $\psi_{sL} - \psi_{s0}$, where ψ_{s0} and ψ_{sL} are the surface potential values at the source and drain side, respectively. These values can be calculated from Eq. (2) by replacing V_{ch} with V_{SB} or V_{DB}, respectively. In weak inversion, the equalities $\psi_{s0} = \psi_{sL} = \psi_{s_{wi}}$ are expected [5]. This implies that even a very small error in the values of ψ_{s0} and ψ_{sL} will result in a large relative error in the difference $\psi_{sL} - \psi_{s0}$, and thus in an anomalous drift current in the mentioned region. The weak inversion values of ψ_{s0} and ψ_{sL}, calculated from the five different expressions, are presented in Table 4. The order of the difference $\psi_{sL} - \psi_{s0}$ obtained

Table 4 Values of weak inversion surface potential at source and drain end obtained when using five different expressions

Express.	ψ_{s0}	ψ_{sL}	$\psi_{sL} - \psi_{s0}$
Eq. (3)	0.79269363564	0.79269363564	0.00×10^{0}
Eq. (1)	0.79265384008	0.79269363564	3.98×10^{-5}
Eq. (2)	0.79250778362	0.79269120772	1.83×10^{-4}
[$\varepsilon = 0.02$]			
Eq. (2)	0.79263695334	0.79269363563	5.67×10^{-5}
[ε_m]			
Eq. (2)	0.79269361362	0.79269363564	2.20×10^{-8}
[ε_{GL}]			

Device parameters are: MOSFET A with $V_{SB} = 0$ V, $V_{DS} = 1$ V, $V_G = 0.25$ V

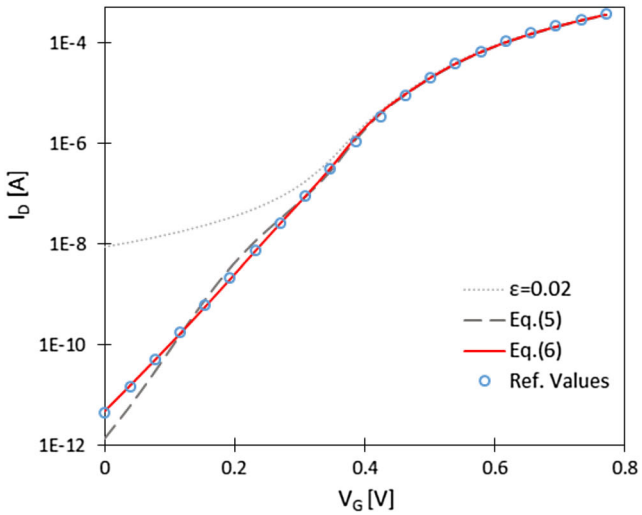

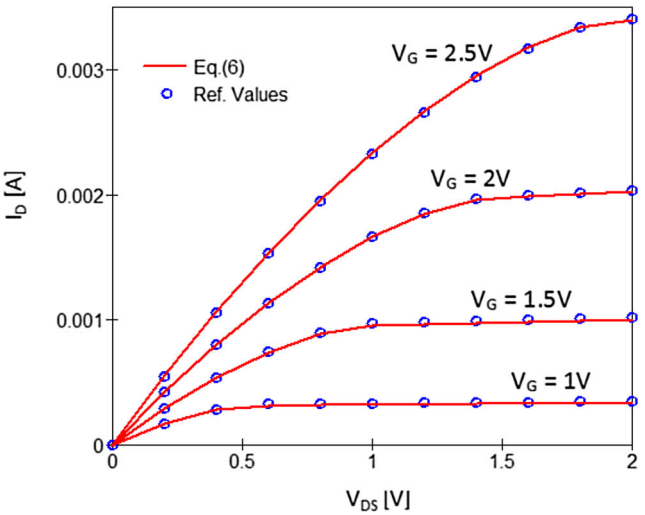

Fig. 4 *Left plot* drain current I_D versus gate voltage V_G using surface potential values obtained from Eq. (1) (*dots*) and Eq. (2) with $\varepsilon = 0.02$ (*dotted line*), as well as with ε_m (*dashed line*) and ε_{GL} (*solid line*), on logarithmic scale. *Right plot* drain current I_D versus drain–source voltage V_{DS} for various values of gate voltage V_G. Device parameters for MOSFET A are given in Table 1

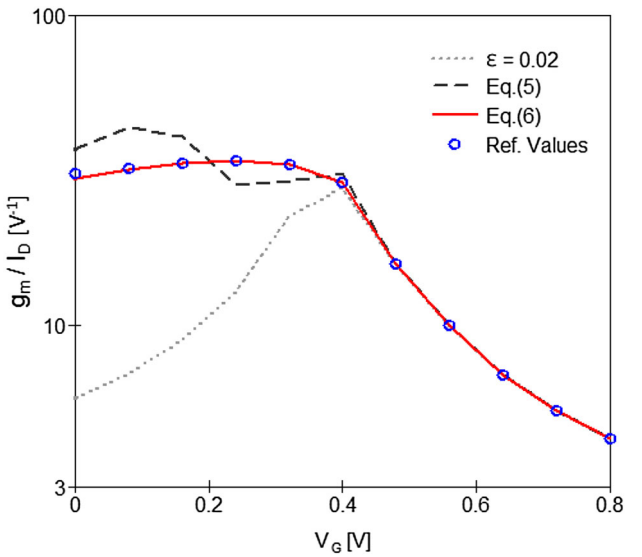

Fig. 5 Ratio g_m/I_D as function of gate voltage using surface potential values obtained from the implicit relation (1) (*circles*) and from the explicit approximation (2) with ε given by Eq. (6) (*solid line*), Eq. (5) (*dashed line*), or a constant value of 0.02 (*dotted line*). Device parameters the same as in Fig. 4

by using the GL-fit factor ε_{GL} (bottom row), is 10^{-8}, much smaller than for those predicted using the original explicit SPB model with constant $\varepsilon = 0.02$ [4] or the SPB model with ε_m modified by Eq. (5) as proposed in [10].

Again, adopting the gradual channel and charge sheet approximations, the drain current (I_D) can be written as the sum of the drift and diffusion components [4]. The drain current was calculated using the surface potential values obtained from the implicit relation (1) and the explicit approximation (2). The smoothing factor ε in Eq. (2) was replaced by a constant value of 0.02, as well as by Eqs. (5) and (6). The left plot in Fig. 4 illustrates the drain current I_D versus gate voltage V_G. As one can see, the most accurate results (compared with the numerical ones) are obtained in the case of the GL-fit factor ε_{GL}. Equation (2) with Eq. (6) for the smoothing factor was implemented in a Verilog A compact model code and simulated in QucsStudio simulator [13,14]. The simulated output characteristics for MOSFET A are shown in the right plot in Fig. 4. This figure also shows the reference output characteristics for MOSFET A for comparison. Since the explicit SPBM with ε_{GL} has good mathematical continuity, the obtained simulation results have fast convergence. The computation time was 0.372 s, being shorter compared with some other models [6,13].

Figure 5 shows a log plot of the transconductance-to-current ratio g_m/I_D as a function of gate voltage when using the explicit and implicit relations for the surface potential. In the explicit relation (2), instead of the smoothing factor ε, we used a constant value of 0.02, as well as Eqs. (5) and (6), respectively. As one can see, the curve obtained from the explicit SPB model with ε_{GL} in the weak inversion region is closer to the reference curve than those obtained with ε_m or the constant value of 0.02. These curves prove the validity of introducing the GL functional form for the smoothing factor into the original explicit SPB model.

7 Conclusions

Implementation of the GL-fit function in the original explicit SPBM leads to an accurate description of the surface poten-

tial over the whole useful range of MOSFET operation. The GL-modified smoothing factor was incorporated into the mentioned SPBM [4] instead of the constant value of 0.02 V and was found to provide a more accurate and continuous description of the drain current from the weak to strong inversion region. Also, more accurate modeling of the transconductance-to-current ratio in the subthreshold region was achieved. Furthermore, the described procedure can be extended to the case where quantum-mechanical effects begin to play a more prominent role in governing the behavior of the device [15–18]. The improvement reported herein was established by comparison with full numerical solutions for different advanced CMOS technologies.

References

1. Pregaldini, F., et al.: An advanced explicit surface potential model physically accounting for the quantization effect in deep-submicron MOSFETs. Solid-State Electron. **48**, 427–435 (2004)
2. Eftimie, S., Rusu, A.: MOSFET model with simple extraction procedures suitable for sensitive analog simulations. Rom. J. Inf. Sci. Tech. **10**, 189–197 (2007)
3. Kumar, M., et al.: Approaches to nanoscale MOSFET compact modeling using surface potential based models, 14th International Workshop on the Physics of Semiconductor Devices. Mumbai, India, December (2007)
4. van Langevelde, R., Klaassen, F.: An explicit surface-potential-based MOSFET model for circuit simulation. Solid-State Electron. **44**, 409–418 (2000)
5. Chen, T.L., Gildenblat, G.: Analytical approximation for the MOSFET surface potential. Solid-State Electron. **45**, 335–339 (2001)
6. Hossain, M., Chowdhury, M.H.: Comprehensive doping scheme for MOSFETs in ultra-low-power subthreshold circuit design. Microelectron. J. **52**, 73–79 (2016)
7. Sharan, N., Mahapatra, S.: Continuity equation based nonquasi-static charge model for independent double gate MOSFET. J. Comput. Electron. **13**(2), 353–359 (2014)
8. Arora, N.D.: MOSFET models for VLSI circuit simulation. Springer-Verlag, New York (1993)
9. Enz, C.C., et al.: An Analytical MOS transistor model valid in all regions of operation and dedicated to low-voltage and low-current applications. Analog. Integr. Circ. S. **8**, 83–114 (1995)
10. Basu, D., Dutta, A.: An explicit surface-potential-based MOSFET model incorporating the quantum mechanical effects. Solid-State Electron. **50**, 1299–1309 (2006)
11. Kevkić, T. et al.; An improved charge-based MOSFET model with parameterized-logistic fiting functions, Proceed. of 24th International Conference ERK 2015, Vol: A, pp. 15-18. Portorož, Slovenia (2015)
12. Jukić, D., Scitovski, R.: Solution of the least-squares problem for logistic function. J. Comput. Appl. Math. **156**(1), 159–177 (2003)
13. Osrečki, Ž.; Compact MOSFET Model (thesis), University of Zagreb (2015)
14. Brinson, M.E., Margraf, M.: Verilog-A Compact Semiconductor Device Modelling and Circuit Macromodelling with the QucsStudio-ADMS Turn-Key Modelling System. Int. J. Microelectron. Comp. Sci. **3**(1), 32–40 (2012)
15. Sho, S., et al.: A simulation study of short channel effects with a QET model based on FermiDirac statistics and nonparabolicity for high-mobility MOSFETs. J. Comput. Electron. **15**, 76–83 (2016)
16. Lizzit, D. et al.; Performance benchmarking and effective channel length for nanoscale InAs, In0.53 Ga0.47As, and sSi n-MOSFETs, IEEE Trans. Electron. Devices, 61, pp. 2027-2034 (2014)
17. Moreau, M., et al.: Simulation study of shortchannel effects and quantum confinement in double-gate FinFET devices with high-mobility materials. Microelectron. Eng. **88**, 366–369 (2011)
18. Mälureanu, E -S.:New approach in determining the tunnelling coefficient for a triangular barrier in MIM junctions, U.P.B. Sci. Bull., Series A, 76, no. 2, pp. 251-262 (2014)